Dynamics of Pipeline Spans Created by ZRB Buckle Triggers: Analytical Approximation

Ralf Peek

Abstract

Zero-Radius Bend (ZRB) buckle triggers provide a reliable means to accommodate thermal expansion of pipelines by triggering sufficiently closely spaced lateral buckles so that none of the buckles ends up absorbing too much thermal expansion. However, it also creates a span to each side of the ZRB support, which may grow due to scour. The same Rayleigh-Ritz approximation that has been successful in accounting for arch action for the first vertical mode of a single span is used to account for lateral arch action for a ZRB span affected by the lateral buckle that forms on the ZRB support. The accuracy of the results for the first horizontal mode is compared with that from FE analysis. It is found that the frictional axial resistance at the ZRB support has an important influence on the natural frequency and damping ratio.

Key Words: Pipeline, Span, ZRB, Lateral Buckle, VIV, Dynamics

1 Introduction

ZRB lateral buckle triggers were invented by the author in 2004, motivated by need for a high-temperature, high-pressure, CRA-clad pipe on a soft clay seabed. The Corrosion Resistant Alloy ("CRA") internal cladding of the pipe requires CRA consumables for the girth welds. The yield strength of such consumables typically undermatches that of the carbon steel carrier pipe. This can result in limited tolerance for bending strains at lateral buckles which form due to thermal expansion. Further, there was considerable uncertainty and variability in lateral-pipe soil interaction: on one hand, the lateral resistance may be too low to reliably lay a curve on the seabed with sufficiently tight radius of curvature to trigger lateral buckling, on the other hand a high lateral resistance could develop after installation and hydrotesting that prevents buckles from forming, and/or causes higher stresses and strains in those that do form.

The ZRB method ensures that buckles will be triggered at a low axial force. Thus, one can guarantee buckle formation at a sufficiently close spacing so that no one buckle becomes overstressed because it accommodates too much thermal expansion.

Sleepers had already been used to trigger buckles when ZRBs were invented. Typically these consist of a pipe horizontal length of pipe that is placed horizontally across the pipeline route and raised slightly above the seabed by a support structure. The pipe is then laid over this sleeper. Under thermal compression, the tendency is for it to upheaval buckle, but before that happens the pipe-sleeper vertical reaction and associated lateral frictional resistance become so small that a lateral buckle develops. Typically the sleeper is also made long enough so the pipe remains on the sleeper when it buckles laterally, which reduces the effect of pipe-soil interaction uncertainty on the pipe stresses and strains due to lateral buckling.

The ZRB trigger structure also consists of a sleeper. However there is a post on one side of the sleeper, as shown in Figure 1 and Figure 2. This allows the lay barge to move as if it were laying a Zero-Radius Bend ("ZRB") on the sleeper thereby wrapping the pipe around the post. It results in a concentration of initial lateral out of straightness on the sleeper which has proven very effective in triggering lateral buckles [1], as had been predicted by the simple analytical methods that motivated the invention and were finally published in [2] together with finite element ("FE") analyses to verify the analytical approximations. Searching "ZRB pipeline" on the web reveals that the method has received considerable attention since its invention, as well as providing pictures and videos animating finite element ("FE") simulations of the pulling the pipe around the post during installation and subsequent lateral buckling.

The same nonlinear FE models used to simulate installation over the ZRB support, and subsequent lateral buckling are also used to calculate the free vibration modes that are used in the VIV assessments of spans. Such modal analysis is based on linearization of the problem about a static equilibrium configuration, which then gives rise to the linear eigenvalue problem that is solved for the natural frequencies, mode shapes, and associated dynamic stress amplitudes. Normally the tangent stiffness would be used for the modal analysis, but for pipe-soil interaction, the static soil springs are typically replaced by dynamic ones, so that one uses an estimated dynamic soil stiffness rather than a static tangent stiffness. (The static tangent stiffness in an FE analysis can depend very strongly on whether the last static solution increment involved loading or unloading. For instance, if the last increment involved heating, the pipe would have been slipping axially towards the buckle, so that the tangent axial soil spring stiffness would be close to zero. Similar issues can arise for the lateral soil springs, and the frictional resistance between the ZRB support and the pipe.)

Whereas such FE analyses have become a routine part of pipe design and assessment in operation, e.g. to account for increasing span lengths due to scour, the author has not found any analytical solutions for the mode shapes of ZRB spans. Yet, assuming the lengths L of the spans to each side of the ZRB support are the same, the lowest vertical and horizontal mode for the ZRB spans are really just mode 2 of a single span of length $2L$. This mode shape is denoted here by $\phi(x)$, and is given in [3]. It includes the effect of the soil springs and the axial force, but not the "arch action" of [4]. For the ZRB, arch action arises mostly for the horizontal (in line) mode due to lateral rather than vertical out-of-straightness ("OOS") of the static configuration.

For the first vertical (cross flow) mode of a single span, the Rayleigh-Ritz approximation in [4] has been found to be quite accurate in capturing arch action, as verified by FE analysis. Both of the following are required for the increase in natural frequency due to arch action: (1) vertical OOS of the static profile similar to that of an inverted arch rather than a straight beam, and (2) axial restraint at the abutments (referred to as "span shoulders"). Absence of one or the other means no arch action and a natural frequency essentially equal to that of a straight beam.

Similar success is achieved here, by applying the same Rayleigh-Ritz approximation to the first lateral (in line) mode of a ZRB span, considering the lateral arch action associated with the lateral buckle that forms the ZRB support. Axial restraint is crucial in developing the arch action, and for the ZRB spans, this must include the axial restraint by friction at the ZRB support. Without this axial friction, there is no lateral arch action and the natural frequency and mode shape is essentially that for mode 2 of a straight span of length $2L$.

The advantages of the analytical solution presented include: (1) It is simple, any static OOS can easily be accounted for, and this can be done by directly using the survey data. (2) The sensitivity to the dynamic axial spring stiffness at the ZRB support is easily calculated, and this can be used to account for amplitude-dependence of the effective support stiffness and damping ratio.

It will be seen than even at low amplitudes of horizontal (in line) vibrations, the axial force at the ZRB support reaches the frictional resistance. This makes for a decrease in natural frequency with increasing amplitudes, as lateral arch stiffness is lost. However, there is also an important increase in energy dissipation by the axial frictional sliding at the ZRB support.

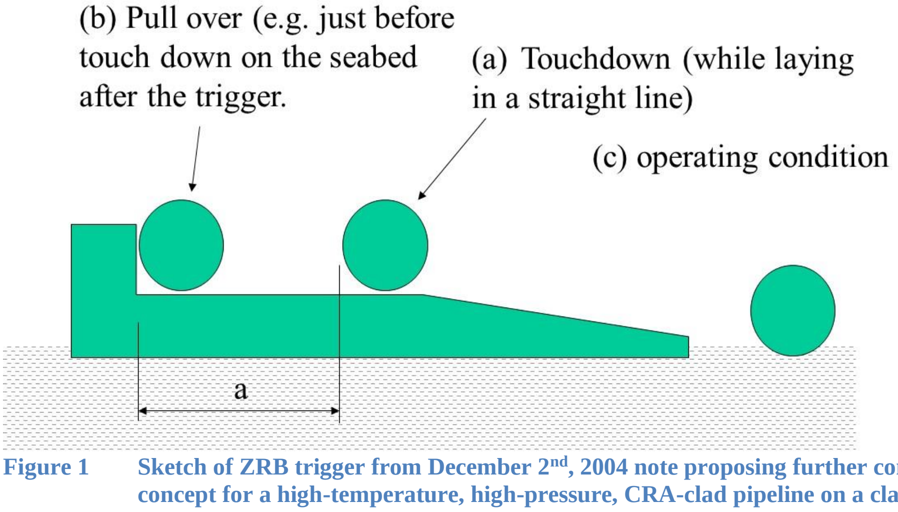

Figure 1 **Sketch of ZRB trigger from December 2nd, 2004 note proposing further consideration of the concept for a high-temperature, high-pressure, CRA-clad pipeline on a clay seabed on the South China Sea. The original 2004 caption: "Cross section of a trigger, showing location of pipe at various stages of laying through to operation. (It is also possible to extend the trigger**

so that the pipe remains on the trigger during operation. This has the advantage a possibly high resistance to lateral movement from the soil is avoided, but it also creates a span.)"

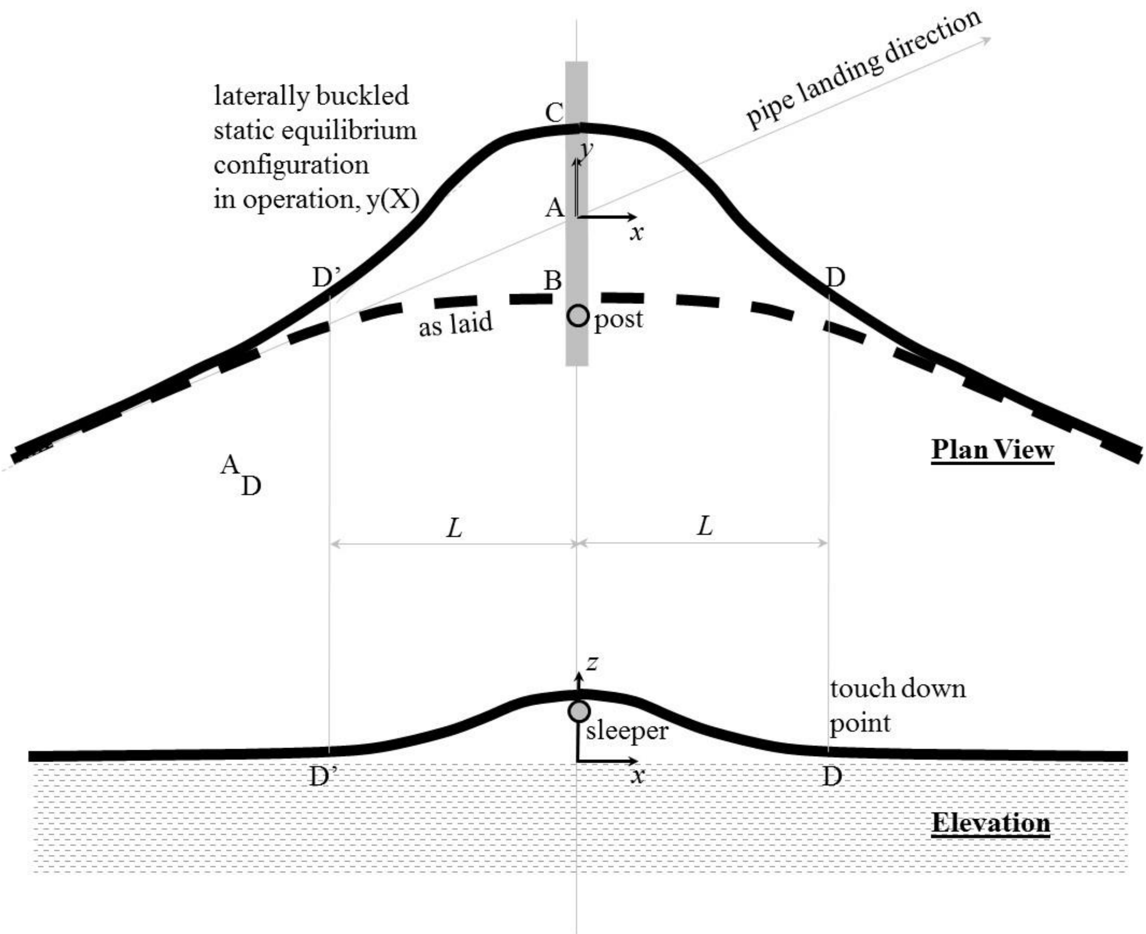

Figure 2 ZRB trigger with coordinate system used

2 Nomenclature

All symbols are defined where they are first used but for convenience key notation is also summarized here.

Symbols

A	=	amplitude of vibration at the point X where it is largest
EA	=	axial rigidity of the pipe
EI	=	flexural rigidity of the pipe
f	=	natural frequency of the ZRB span for the first lateral mode including arch action (in cycles per unit time)
f_u	=	natural frequency of the ZRB span for the first lateral mode without arch action. Also equal to the frequency of the 2nd mode for a span of length 2L; given in [3].
k_x, k_y, k_z	=	for $\lvert x\rvert \geq L$, these are the dynamic soil spring stiffnesses in the axial (x), lateral (y), and vertical (z) directions; otherwise zero
L	=	span length from ZRB support to touch down point (Figure 2), assumed to be the same on both sides
L_{EA}	=	equivalent axial restraint length for the dynamic response; in regard to axial restraint, the pipe behaves as if it were axially fully fixed at the ZRB support, then axially fully free until a distance L_{EA} from the support, where it is again fully fixed

N, Q, M = effective axial force, shear force, and bending moment for two-dimensional (2D) case (Figure 3); for three-dimensional (3D) case, see text following (4)

u,v,w = displacements of the centroid of the pipe from the initial to the current configuration

x,y,z = cartesian coordinates in the axial, lateral and vertical upwards direction (Figure 2)

X,Y,Z = coordinates of a material point at the centroid of the pipe in the initial configuration; X is also equal to the x coordinate of the same material point in the reference configuration

λ_x = characteristic length with which N_d and u_d decay exponentially away from the spans. See (14) to (16).

$\phi=\phi(x)$ = mode shape for 2nd mode of a single span of length $2L$; also shown to be equal to the mode shape for the ZRB span if axially unrestrained; provided in [3]

ξ = material or component damping ratio

ζ = modal damping ratio or contribution of a component to the modal damping ratio

$\int_{(.)}$ = depending on whether (.) is a statement or a set this means the integral over all X for which (.) is true, or over all $X \in (.)$

Subscripts

$(.)_0$ = refers to (.) evaluated at X=0

$(.)_a$ = value of (.) associated with arch action, or contribution due to arch action

$(.)_b$ = refers to contribution to (.) from the seabed

$(.)_d$ = dynamic value of (.), change in (.) from static equilibrium configuration about which small-amplitude vibrations take place, modal value of (.) associated with the free vibration mode shape

$(.)_B$ = refers to contribution to (.) from the ZRB support

$(.)_p$ = refers to contribution to (.) from the pipe

$(.)_r$ = refers to the value of (.) in the right span ($0 < X < L$) for a quantity that is constant within that zone

$(.)_s$ = value of (.) for the static equilibrium configuration about which small amplitude vibrations take place

3 Theory

Both the FE analysis results as well as the analytical ones in this paper are based on a geometrically nonlinear beam theory that employs the same approximations used by Von Kármán in his analysis of buckling of plates shells. For the 2D case, the governing equations are:

$$Q' + q + (N\,y')' = 0,\quad N' + p = 0,\quad Q = M' \tag{1}$$

$$M = EI\,\kappa,\quad N = EA\,\epsilon + N_T\,,\quad \kappa = (y - Y)'',\quad \epsilon = x' - X' + \tfrac{1}{2}\,y'^2 - \tfrac{1}{2}\,Y'^2 \tag{2}$$

In the above, three pipe configurations are considered: (1) a reference configuration in which the centroid of the pipe cross section is on the x axis, (2) an initial stress-free configuration, and (3) the current (loaded) configuration. A point at $(X,0)$ in the reference configuration, moves to $(X,Y(X))$ in the initial configuration, and further to $(x(X,t),y(X,t))$ in the current configuration. This sequence of positions and be written as:

$$(X,0) \rightarrow (X,Y(X)) \rightarrow (x(X,t),y(X,t)) \tag{3}$$

Further, N, Q, and M are the stress resultants at a cross section as shown in Figure 3 (axial force, shear force and the bending moment, respectively), finally N_T denotes the axial force due to operating temperature and pressure under axially constrained conditions. All quantities are written as functions of X, and a prime denotes differentiation with respect to X. Further p and q are the distributed forces per unit length acting in the pipe in the x and y directions, respectively, and these include any force the seabed exerts on the pipe.

Under water, it is not convenient to apply equations (1) and (2) exactly as stated. Instead, the same equations may be applied after: (a) reinterpreting N and N_T as effective axial forces, (b) replacing the external pressure contributions to p and q by a buoyant force equal to the weight of water displaced by the pipe acting in the vertically upward direction, and (c) interpreting the "stress free" conditions for the initial configuration to mean that N=Q=M=0 everywhere for the reinterpreted N with the external pressure applied.

As stated, (1) and (2) are for static analysis, but they can be applied for dynamic analysis if one replaces p and q by $p - m_p \ddot{x}$ and $q - m_{eff} \ddot{y}$, respectively, where m_p denotes the mass per unit length of the pipe, coatings and contents, and $m_{eff} = m_p + c_a\, m_{dw}$ is the effective mass, m_{dw} the mass per unit length of water that is displaced by the pipe and c_a the added mass coefficient, given by c_a=1 for irrotational flow theory without seabed proximity effects. There can also be drag and other hydrodynamic forces but these are neglected here, by considering only small amplitude vibrations of the pipe in still water.

For the 3D case, (3) becomes

$$(X,0,0) \rightarrow (X,Y(X),Z(X)) \rightarrow (x(X,t),y(X,t),z(X,t)) \tag{4}$$

and (1) and (2) can also be applied after replacing M, N, Q, q, y, Y and κ by vectors in the y-z plane denoted by $\mathbf{M}$, $\mathbf{N}$, $\mathbf{Q}$, $\mathbf{q}$, $\mathbf{y}$, $\mathbf{Y}$ and $\boldsymbol{\kappa}$, respectively. Further, y'^2 and Y'^2 are replaced by the dot products $\mathbf{y}'.\mathbf{y}' = y'^2 + z'^2$ and $\mathbf{Y}'.\mathbf{Y}' = Y'^2 + Z'^2$, respectively, and Figure 3 may be applied to projections pipe and the forces onto the vertical x-z plane as well as the horizontal x-y plane.

This Von Kármán, moderate-displacements theory does include nonlinear effects, and is quite successful at capturing buckling phenomena, but it is an approximation, valid for small rotations $\theta \cong -y' \cong \sin(\theta) \cong \tan(\theta)$. It is also consistent, in the sense that the equilibrium equations (1) may be derived from the kinematics (2) as well as from approximate equilibrium of the element of pipe as shown in Figure 3.

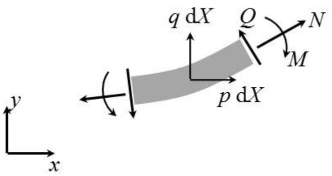

Figure 3 Forces in the current configuration on an element of pipe of length dX in the reference configuration.

For the analytical results presented, the rotation θ of the cross sections is $\theta = -v'$ so that sections normal to the pipe remain normal, but for the FE analysis, shear deformations are allowed, with the shear strain given by $\gamma = \theta + v'$, the curvature κ replaced by the rate of change of the rotation of the cross sections $\kappa = \theta'$, and the shear force obtained from $Q = GA_s\,\gamma$, where G is the shear modulus of the pipe steel and A_s the shear area, taken as half the cross sectional area of steel.

Although (2) contains a nonlinear term, it still leads to a linear problem if (a) the pipe is axially unrestrained everywhere (i.e. p=0) except at one point, (b) axial inertia $m_p\, \ddot{u}$ is negligible, and (c) the same axial force $\bar{N}$ is applied at both ends. It then readily follows from (1) and (2) that

$$N = \bar{N} \;\; \forall\, X, \qquad EI\,(y - Y)'''' - N\, y'' + m_{eff}\, \ddot{y} = q \tag{5}$$

which is a linear in the only unknown, $y=y(X,t)$.

For a dynamic increment in lateral displacement v_d superposed on a static equilibrium configuration and dynamic soil springs of stiffness k_y where the pipe is in contact with the seabed, and $k_y = 0$ in the spans, the governing equation becomes

$$EI\, v_d'''' - N\, v_d'' + k_y\, v_d + m_{eff}\, \ddot{v}_d = 0 \tag{6}$$

I.e., it does not matter whether the static equilibrium configuration is straight or curved, provided that the pipe is axially unrestrained and axial inertia negligible, the governing equation for the dynamic increment is the same as for a straight pipe. Further, the 2nd mode $v_d = \phi(X)\ \sin(2\pi f_u t)$ for a single span of length $2L$ (extending over $X \in [-L,L]$) is known [3], it is antisymmetric, and therefore zero at x=0. Thus, $\phi(X)$ satisfies the boundary condition for the lateral restraint at X=0 provided by the ZRB support. Axial restraint at the ZRB support also does not invalidate the solution provided that it is the only point with axial restraint. The natural frequency of this axially unconstrained mode $\phi(X)$ is denoted by f_u. Both are given in [3], and therefore not repeated here, except that the particular values will be given for the numerical example that follows. (The same solution can also be calculated as described in [4], if one replaces "$L/2$" by "L", and "cosh" in the expression for "f_1" by sinh, and "cos" in the expression for "f_2" by sin.)

In reality, there is axial restraint from the seabed as well as the ZRB support, and this is what gives rise to lateral arch action. To account for this, the same Rayleigh-Ritz as in [4] is used: For assumed lateral dynamic displacements $v_d = \phi(X)$ from the axially unconstrained mode, a static equilibrium problem is solved for the axial direction. This then leads to a dynamic axial force $N_d(X)$ and axial displacement $u_d(X)$. Here "dynamic" means a small dynamic increment added to the static equilibrium configuration. As in any modal analysis, the dynamic equations are obtained by linearization about a static equilibrium configuration. In view of the linearization, only the leading order term in $\phi(X)$ is retained. The axial potential energy can then be written as

$$\Pi_a = \Pi_{ap} + \Pi_{aB} + \Pi_{ab} \tag{7}$$

$$\Pi_{ap} = \int_{(-\infty,\infty)} ½\ N_d^2/EA\ dX,\ \ \Pi_{aB} = ½\ K_x\ [u_d]_{x=0}{}^2\ ,\quad \Pi_{ab} = \int_{|X|\geq L}\ ½\ k_x\ u_d^2\ dX \tag{8}$$

where Π_{ap}, Π_{aB}, and Π_{ab} are the contributions to the potential energy from axial stiffness of the pipe, that of the axial spring at the ZRB support, and that of the axial soil springs on the seabed, respectively; K_x denotes the dynamic stiffness for the axial restraint at the ZRB support, and k_x denotes the dynamic stiffness of the axial soil springs or zero for $x \in (-L,L)$. The subscripts after the integration signs are either a set in which case integration is over all X in that set, or a statement in which case integration is over all X for which the statement is true.

These potential energy values for undamped, single-mode response represent the maximum potential energy, which occurs when the displacement at any given point is at a maximum or minimum and the velocity is zero. It must be equal to the kinetic energy when the velocity is at a maximum or minimum and the displacements are zero. Writing this energy balance condition for the axially restrained and unrestrained cases yields

$$\Pi_u = ½\ (2\pi f_u\ \phi)^2\ M,\quad \Pi_a + \Pi_u = ½\ (2\pi f\ \phi)^2\ M,\quad M = \int_{(-\infty,\infty)} m_{eff}\ \phi^2\ dx \tag{9}$$

respectively. In both equations, the left hand side represents the potential energy when the dynamic displacements are at a maximum and the velocity is zero, whereas the right side represents the kinetic energy when the velocity is at a maximum and the velocity is zero. Further, Π_u denotes the potential energy for the axially unconstrained case, and f denotes the natural frequency including arch action. Eliminating Π_u then yields

$$f = (f_u^2 + f_a^2)^{1/2},\quad f_a = (2\Pi_a/M)^{1/2}/(2\pi) \tag{10}$$

It only remains to calculate the solution N_d=$N_d(X)$ and u_d=$u_d(X)$ to the static equations for the axial (x) direction. For this, it is assumed that the static equilibrium configuration about which the vibrations take place is available, it is denoted by $(x_s(X),y_s(X))$, and it must satisfy the governing conditions (1) and (2). Adding dynamic displacements (u_d(X), v_d(X)=$\phi(X)$), the configuration becomes (x,y)=$(x_s+u_d,\ y_s+v_d)$. Looking at the change in the 2nd equation in (1) and the 2nd and 4th equations in (2), retaining only leading-order terms in ϕ, and noting that the dynamic value of force per unit length that the seabed exerts on the pipe is $p_d = -k_x\ u_d$ where k_x is the axial dynamic soil spring stiffness due to the dynamic portion yields

$$N_d' = k_x\ u_d,\quad N_d = EA\ \epsilon_d\ ,\ \ \epsilon_d = EA\ (\ u_d' + y_s'\ \phi') \tag{11}$$

The boundary conditions are N_d, $u_d \to 0$ as $|X| \to \infty$, and axial equilibrium of an infinitesimal element of pipe on the ZRB support (at X=0) yields that there must be a change in N_d moving across the support in the positive x direction by an amount $K_x\, u_d$, which arises from the force that the axial spring at the ZRB support exerts on the pipe.

The above are the equations for a straight pipe restrained by a concentrated spring K_x at X=0 and by distributed springs k_x for $|X| \geq L$ subject to a thermal contraction $y_s'\,\phi'$. Most of this thermal contraction $y_s'\,\phi'$ occurs within the spans ($|x| < L$), and there k_x=0, so that N_d must be constant except for the discontinuity x=0. As an approximation, it is assumed that all the $y_s'\,\phi'$ occurs within the span. The total contraction in the right ($X \geq 0$) span is then

$$g_d = \int_{[0,\infty)} y_s'\,\phi'\, dX = \int_{[0,\infty)} (y_{s0} - y_s)\,\phi''\, dX \tag{12}$$

where y_{s0} denotes the value of y_s evaluated at x=0. The other side experiences an expansion by the same amount. Therefore g_d also represents the axial dynamic displacement that would develop at the ZRB support if the pipe is axially unrestrained there. The second form of the integral in (12) has been added so that y_s=$y_s(X)$ need not be differentiated if it is obtained from survey data, or from a quasi-static finite element analysis. It is also worth noting that

$$\int_{[0,\infty)} X\,\phi''\, dX = 0 \tag{13}$$

which means that when g_d is calculated from survey data, the result will not be sensitive to the exact choice for the direction of the x axis.

Completing the solution of the axial problem for the case the static profile y_s=$y_s(X)$ is symmetric yields that u_d is symmetric and N_d is antisymmetric, and for X>0 these are given by

$$N_d = N_{dr} \text{ for } X\in(0,L),\;\; N_d = N_{dr} \exp[-(X\text{-}L)/\lambda_x] \text{ for } X>L \tag{14}$$

$$u_d = 2N_{dr}/K_x \text{ at } X\text{=}0,\;\; u_d = -(N_{dr}/\lambda_x k_x) \exp[-(X\text{-}L)/\lambda_x] \text{ for } X>L \tag{15}$$

where

$$N_{dr} = EA\, g_d/L_{EA}\,,\quad L_{EA} = 2EA/K_x + L+\lambda_x,\quad \lambda_x = (EA/k_x)^{1/2} \tag{16}$$

Substituting (14) and (15) into (8) and evaluating the integrals yields

$$\Pi_a = \Pi_{ap} + \Pi_{ab} + \Pi_{aB} \tag{17}$$

where

$$\Pi_{ap}=LN_{dr}^2/EA+\Pi_{ab},\;\; \Pi_{ab} = ½\, \lambda_x N_{dr}^2/EA,\;\; \Pi_{aB} = 2\, N_{dr}^2/K_x \tag{18}$$

are the contributions to the potential energy due to arch action Π_a from axial deformations of the pipe (subscript "p"), the distributed axial soil springs on the seabed ("b"), and the concentrated axial soil spring at the ZRB support ("B"), respectively. Equations (10) and (16) to (18) can be combined to yield

$$\Pi_a = EA\, g_d^2/L_{EA}\,,\quad f_a = g_d\,[2\, EA/(L_{EA}\, M)]^{1/2} \tag{19}$$

Thus, all that needs to be done to get the natural frequency including arch action is calculate the following in the order stated: M from (10), g_d from (12), f_a from (19), and finally f from (10).

Perhaps even more important than the effect of lateral arch action on the natural frequency of the in line mode is that on the damping ratio. Every structural element or component that contributes to the potential energy and stiffness (such as the axial spring to represent the ZRB support) will in general also contribute to the damping. To account for this, it is assumed, as in [4] and in Section 4.6 of [5], that the energy dissipated per cycle by a component is equal to $4\pi\xi$ times the maximum potential energy of the component, where ξ is the material or component damping ratio. For linear viscous damping, ξ is constant with respect to amplitude, and proportional to frequency. However, for spans structural and soil damping is typically not viscous, and it is necessary to estimate ξ for the amplitude and frequency that is expected.

To calculate the contribution of a component to the modal damping ratio ζ, one simply multiplies the ξ value by the fraction of the total potential energy of vibration attributed to that component. Each of the contributions to Π_a from (18) or (8) can be viewed as a component with its own ξ value. Thus, the components are axial deformations of the pipe (ap), the axial soil springs on the seabed (ab), and the axial spring for the ZRB support (aB). Combining these to get the contribution to the modal damping from arch action yields

$$\zeta_a = \zeta_{ap} + \zeta_{ab} + \zeta_{aB},\ \ \zeta_{ap} = \xi_{ap}\, \Pi_{ap}/\Pi,\ \ \ldots,\ \ \ \Pi = ½\, M\, (2\pi f)^2 \tag{20}$$

The values for the numerical example are summarized on Table 1. Similarly, the contributions to modal damping from flexural deformations of the pipe ζ_{fp} and the lateral soil springs ζ_{yb} may be calculated using

$$\Pi_{fp} = ½ \int_{(-\infty,\infty)} EI\, \phi''^2\, \mathrm{d}X,\ \ \ \Pi_{yb} = ½ \int_{|X|\geq L} k_y\, \phi^2\, \mathrm{d}X \tag{21}$$

There is one other component of potential energy that is required to complete the balance between potential and kinetic energy: it is associated with the static axial force N_s and denoted by Π_N. However, for reasons given in [4] that component does not have any damping associated with it for small amplitude vibrations. The energy balance conditions then become

$$\Pi = \Pi_u + \Pi_a,\ \ \ \Pi_u = \Pi_{fp} + \Pi_{yb} + \Pi_N\ ,\ \ \ \Pi_N = ½ \int_{(-\infty,\infty)} N_s\, \phi'^2\, \mathrm{d}X \tag{22}$$

4 Numerical Example

4.1 Definition (Inputs)

The intent here has been to create an example that is simple enough to enable a compact description that makes it fully reproducible, yet realistic. However, it is only intended for illustration, and inputs used should not be interpreted as recommended values for any particular conditions. A number of the inputs are only needed for the FE model used for this example and not for the analytical one presented.

A 20-inch pipe is considered with an outer diameter of the steel pipe of 0.508m and a wall thickness of 18mm. With the coatings, the outer diameter increases to D=0.594m. The flexural and axial rigidity are given by EI=17.38 MNm^2 and EA=5736 MN. (For simplicity the stiffness of the coatings have been neglected, and they are also not considered in calculating the axial and bending stresses in the steel.) The submerged weight during operation is 1.22 kN/m. For simplicity, the same weight is assumed throughout installation, operation, and shut down. The mass per unit length of the pipe is m_p = 408 kg/m, and including the added mass with c_a=1, the effective mass in the transverse (vertical and lateral) directions is m_{eff} = 692 kg/m.

The ZRB sleeper rises 0.5m above a flat seabed, and is assumed to extend far enough so the pipe does not fall off during lateral buckling. (As a base case, the original ZRB design proposal of Figure 1 envisioned a ZRB support designed to allow the pipe to ramp down to the seabed during lateral buckling to avoid spans, but it appears that most ZRBs installed also support the pipe when buckled, which removes some of the pipe-soil interaction uncertainty for fully formed buckles on the seabed.)

The dynamic soil spring stiffnesses taken as k_x=k_y=k_z= 1 MN/m^2 for all (axial, lateral & vertical) directions, and the associated material damping ratios are taken to be ξ_{ab}=ξ_{yb}= ξ_{zb} = 0.1. For the FE model, static soil spring stiffnesses of 0.24, 0.3, and 0.2 MN/m^2 are used for the *x*, *y* and *z* directions, but these are only activated when the pipe is in contact with the seabed, and friction coefficients of 0.6 and 0.7 are used to allow slip in the *x* and *z* directions, when the force in that direction exceeds the friction coefficient times the normal force. As a result, the mobilization displacement for axial and lateral slip depends on the normal force, and where the normal force is equal to the pipe weight, the penetration into the seabed is 6mm, and the mobilization displacements for the axial and lateral directions are 3mm and 2.8mm, respectively. The lateral and axial soil springs are assumed to act independently of each other.

A similar approach is used to model the ZRB support, with the dynamic stiffness and material damping ratio for all 3 directions, and given by K_x=K_y=K_z=10 MN/m and the corresponding damping ratios are ξ_{aB} = ξ_{yB} = ξ_{zB} = 0.2. The material damping ratios relevant to the analytical model are also summarized in Table 1. The static stiffnesses are 30, 40 and 50 MN/m for the *x*, *y* and *z* directions, respectively, and the friction coefficients are 0.5 for both the axial (*x*) and lateral (*y*) directions.

The post has the same properties as the ZRB sleeper, except that they are rotated by 90°, as would be required to rotate the sleeper to the orientation of the post. It only engages the pipe during installation, and therefore its dynamic properties do not affect the reported results.

Normally points that are midway between two buckle triggers experience very little displacement, and are therefore sometimes termed "virtual anchor points". The pipe model extends between two such points, spaced at 2km with one ZRB included in the middle of the model.

The bottom tension during installation is N_{lay}=0.4MN, and deviation of the lay direction from the x-axis is about α_{lay} = 0.1 radians. Thus the total change in lay direction at the ZRB support is 0.2 radians (11.4°). The landing point on ZRB sleeper is at (x,y)=(0,0) as shown in Figure 2. This refers to the point where the pipe first lands on the sleeper during installation. From there the pipe can move by an amount $\alpha_{lay}\,(EI/N_{lay})^{1/2}$ = 2.08m in the negative y direction during the lateral pull before it engages the post. This is the distance recommended in [2] based on an analytical solution for the pipe wrapped around the post under the lay tension.

Operating conditions are a temperature rise of 60°C above installation conditions with a coefficient of thermal expansion of $\alpha_T = 1.17 \times 10^{-5}$ per °C, and an internal pressure of 15MPa. These are applied, fully removed, and applied again, whereupon the modal analysis is performed for the hot conditions at the 2nd operating cycle.

4.2 FE Model and Static Loading Results

The FE analysis is performed with Npex [6,7], using 2-noded pipe elements based on the nonlinear, small-rotations theory of (1) and (2) with shear deformations included as described between (4) and (5), and with linear interpolation of the displacements and rotation within the element. The element length is 0.5m up to 200m from the ZRB support (where the pipe experiences significant bending in operation) and 5m beyond that.

Pipelay is modeled approximately, but this is not expected to affect the results presented for operating conditions: A simplified, very long "lay barge" is defined as vertical unilateral spring attached to each node. These initially support the pipe at the sea surface, and are then moved downward to simulate the stinger and the forward motion of the lay barge, until eventually they lose contact with the pipe, as they should when the pipe loses contact with the stinger. In the horizontal (x,y) plane, the pipe initially extends from (-1000,-100)m to (1000,100)m, fully supported by the "lay barge" at an elevation of 80m above the seabed. At the start (X=-1000m), at pipe is fixed in the horizontal (x & y) directions, and at the end (X=1000m) forces of 0.4MN and 0.04MN are applied in the x and y directions respectively. This keeps pipe aligned with its initial position. Pipelay then progresses in a straight line, and eventually the pipe lands on the ZRB trigger at (0,0). Thereafter pipelay continues in a straight line until the slope of the vertical pipe profile at the ZRB sleeper is zero. This occurs before touch down at the right (X>0) side of the trigger, as can be seen in Figure 4. Then the lateral pull is simulated by changing the y-component of force at the end of the pipe from 0.04MN to -0.04MN. (All steps are done in a number of small increments, calculating converged solutions of the nonlinear problem for each increment.) Pipelay then continues until all of the lay barge springs have lost contact with the pipe, so the pipe is supported by the seabed everywhere except near the ZRB support. Then the end node is fixed, and 2 operating cycles applied with full (pressure and temperature) unloading between cycles.

The pipe configurations at various stages of the static FE analysis are shown in Figure 4. In the elevation view, the following plots were so close that no differences can be seen: those at the start and end of the lateral pull, the as-laid and cooled configuration at the end of the first operating cycle, and the hot configuration for the 1st and 2nd cycles.

The modal analysis is performed for the 2nd operating cycle with the pipe hot. The results thereof are compared in the next section with those from the analytical solution.

The choice of landing position on the ZRB sleeper, relative to the post has been made based on an analytical result in [2] to end up with a more less symmetric as laid and laterally buckled profiles, and it can be seen from Figure 4 that this was successful.

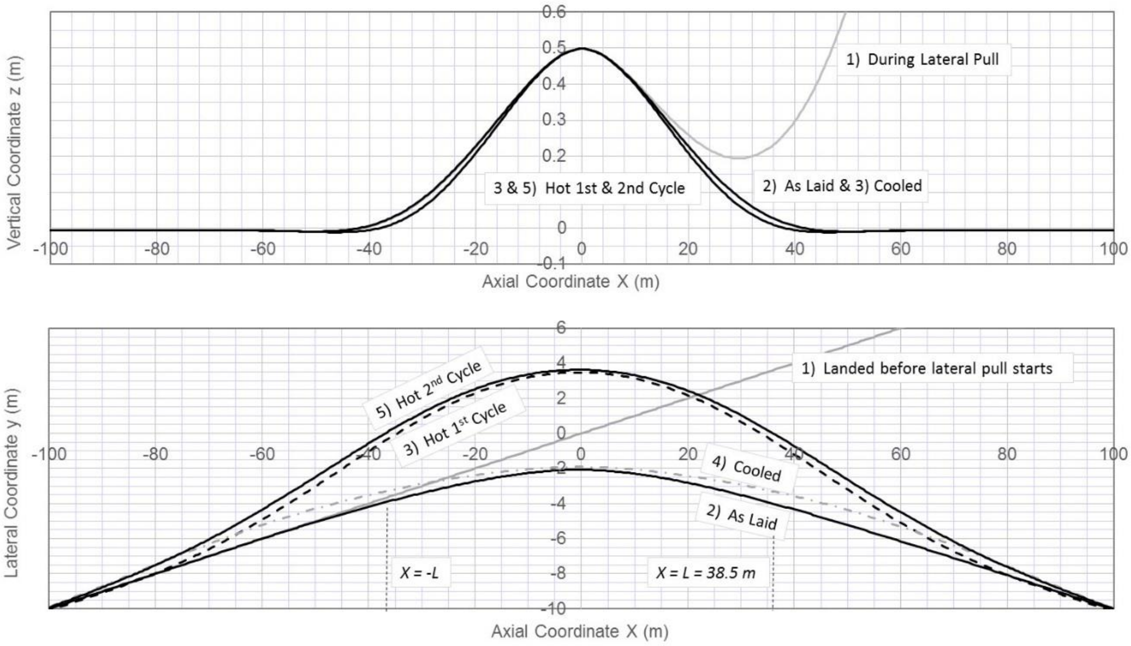

Figure 4 Pipe configuration for different phases of installation and operating conditions

4.3 First Lateral Mode Shape Results from Analytical and FE Models

Results from the static FE analysis that are used in the analytical solution are: the displaced shape $y_s(X)$ from the plan view in Figure 4, the corresponding span length L=38.5m taken as the distance to the first node in contact with the seabed, and the effective axial N_s = -0.315 MN (compression).

The 2nd lateral mode of a straight span of length 2L, which is also the lateral mode for the ZRB span under axially unconstrained conditions, has a natural frequency of f_u = 0.58181 Hz and the mode shape is

$$\begin{aligned} \phi(X) &= C_1 \sinh(aX) + C_2 \sin(bX) && \text{for } 0 \le X \le L \\ &= \exp(-\alpha\,(x-L))\,[C_3 \sin(\beta\,(x-L)) + C_4 \cos(\beta\,(x-L))] && \text{for } X > L \\ &= -\phi(-X) && \text{for } X < 0 \end{aligned} \tag{23}$$

where a=0.080434 m^{-1}, b=0.091088 m^{-1}, α=0.19352 m^{-1}, β=0.19587 m^{-1}, C_1=0.041779, C_2=0.91799, C_3=-0.076861, C_4=0.13330. This mode shape is shown in Figure 5 together with that from the FE analysis. It has been normalized to a maximum modal displacement of 1. (It is envisioned that the modal displacements are dimensionless and multiplied by the dynamic displacement where it largest to get the dynamic displacements everywhere. However, the associated modal stresses (also shown in Figure 5) are multiplied by the outer diameter including the coatings, D, for compatibility with the definition of modal stresses in [8].)

Evaluating of the integrals in (9) and (12) numerically yields M=26.619 Mg and g_d=0.12364 m/m. Equation (16) yields λ_x = 75.735m for the characteristic length with which dynamic axial effects decay away from the span, L_{EA} = 1261.4m for the equivalent axially unconstrained length (in the sense that having the pipe axially fully fixed for $|X| > L_{EA}$ and at X=0, but fully free everywhere else gives the same level of axial constraint, as the axial springs considered), and N_{dr}=0.56220 MN/m for the modal axial force in the right span. The contributions to the modal potential energy Π are shown in Table 1. The total potential energy for arch action from (17) or (19) is Π_a = 69.509 kJ/m^2, which leads to f_a = 0.36371 Hz from (10), and f = 0.68614 Hz for the natural frequency of the span including arch action. This is only 0.25% below the value f = 0.68785 Hz from the FE analysis. It is seen from Figure 5 that the mode shape and modal stresses from the analytical Rayleigh-Ritz approximation are also in good agreement with those from the FE analysis.

The following approximations of the analytical solution should increase the analytical natural frequency: the Rayleigh-Ritz approximation, neglecting axial inertia, and neglecting shear deformations. That the FE natural frequency is higher rather than lower than that of the analytical solution therefore indicates some combination of sources of error in the opposite direction are larger. These could include FE discretization errors, and the slight lack of symmetry in the static equilibrium configuration.

The FE discretization errors arise from the element length of 0.5m, the interpolation of displacements and rotations within each element, and concentrating soil springs a the nodes. Indeed, the span length is only 38.1m if one measures it to where the penetration into the seabed is zero, considering the linear interpolation of displacements within the elements, as opposed to the 38.5m used, based on the distance to the first node that is in contact with the seabed. This makes a difference of 1% in span length, which results in a 1.5% increase in the analytical natural frequency, to a value 1.2% above that of the FE analysis.

Calculating potential energy for each structural component according to (16) and (21), and the associated contributions to the modal damping ratio ζ based on (20) yields the results in Table 1. The total modal damping ratio is $\zeta = 7\%$, 73% of which comes from damping due to axial motions at the ZRB support. This damping ratio is what is referred to in [8] as structural and soil damping. It does not include any hydrodynamic damping, since that is already included in the VIV response functions used in the fatigue calculation.

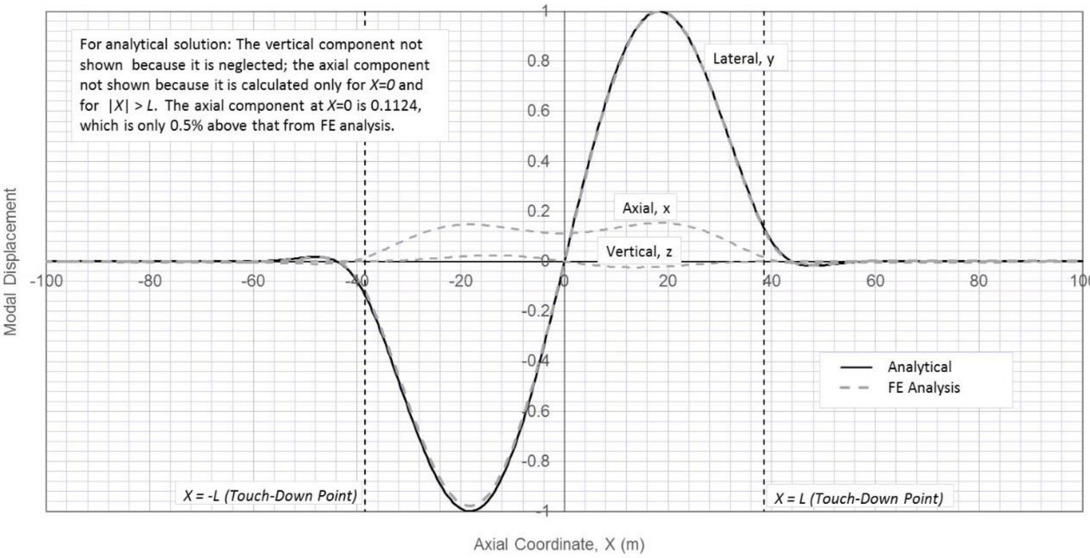

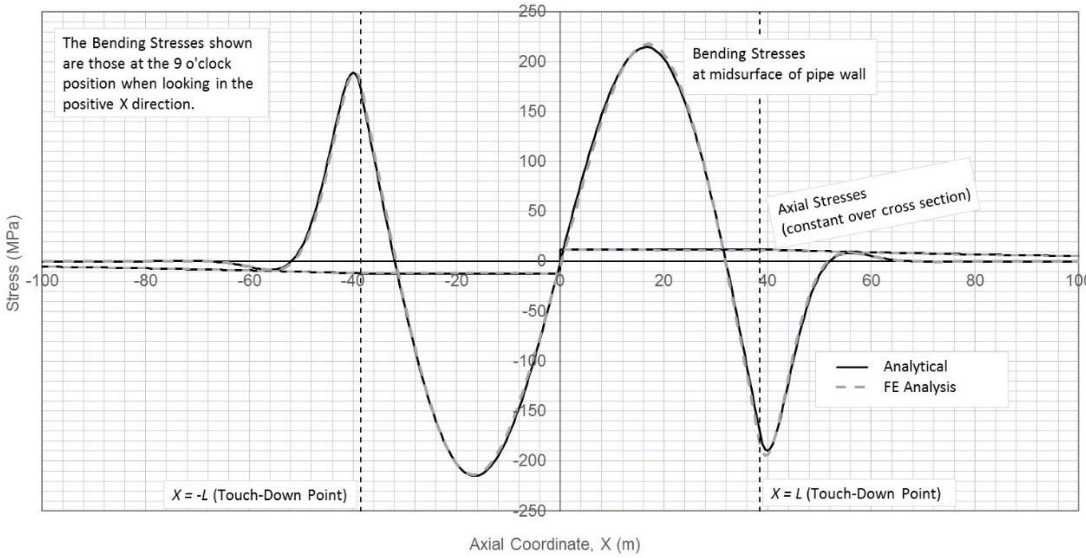

Figure 5 Modal shape and modal stresses for first lateral (in line) mode at maximum amplitude of vibration D from analytical approximation presented and FE analysis

$\Pi_{(.)}$	Component Description & (Eqn. from which it is calculated)	Value (kJ/m^2)	Fraction of Total $\Pi_{(.)}/\Pi$	$\xi_{(.)}$ (input)	$\zeta_{(.)}$
Π_{ab}	Axial Soil Springs on Seabed (18)	2.09	0.84%	10%	0.08%
Π_{aB}	Axial Spring at ZRB support (18)	63.21	25.55%	20%	5.11%
Π_{ap}	Axial Deformation of Pipe (18)	4.21	1.70%	1%	0.02%
Π_{fp}	Flexural Deformation of Pipe (21)	189.11	76.45%	1%	0.76%
Π_{yb}	Lateral Soil Springs on Seabed (21)	24.92	10.07%	10%	1.01%
Π_{N}	Potential Energy of Static Axial force N_s (22)	-36.17	-14.62%	0%	0.00%
Π	Total Potential Energy, sum of above as in (22), also equal to kinetic energy of pipe as in (20)	247.37	100%		6.98%

Table 1 Contributions $\Pi_{(.)}$ to the modal potential energy for each component, the equation from which it is calculated, the value in MJ/m^2, the material damping ratio $\xi_{(.)}$ and the contribution to the modal damping ratio $\zeta_{(.)}$.

5 Discussion – Nonlinearity and Inelasticity of ZRB support

With the analytical model, it is easy to calculate the sensitivity of the results to the dynamic stiffness K_x and damping ratio ξ_{aB} of the ZRB support. In this section that is exploited, to account for the amplitude-dependent equivalent stiffness K_x and damping ratio ξ_{aB} considering the frictional axial slip at the ZRB support.

The vertical reaction at the ZRB support from the FE analysis is 68.88 kN. Assuming a dynamic friction coefficient equal to the static one of $\mu_{aB} = 0.5$, this means that the axial frictional resistance is $F_{maB} = 34.44$ kN, which is assumed to be reached at a mobilization displacement of $u_{maB} = 2$mm. Up to that point linear elastic behavior with a stiffness $K_{xe} = F_{maB}/u_{maB} = 17.22$ MN/m is assumed with no damping. Beyond that point, slip is assumed to occur at constant force.

Following Section 4.6 of [5] and [4], this elastic-perfectly-plastic behavior of the ZRB support can be approximated by a linear spring based on the secant stiffness K_x, and a damping ratio ξ_{aB} equal to the ratio of the energy dissipated per cycle divided by 4π times the elastic strain energy based on the stiffness K_x. Thus one obtains

$$K_x = K_{xe},\quad \xi_{aB} = 0 \quad \text{for } |u_{d0}\,A| \le u_{maB}$$
$$K_x = F_{maB}/|u_{d0}\,A|,\quad \xi_{aB} = (2/\pi)\,(1 - u_{maB}/|u_{d0}\,A|) \quad \text{for } |u_{d0}\,A| > u_{maB} \tag{24}$$

where u_{d0} is the value of the modal displacement $u_d(X)$ evaluated at X=0, and A denotes the amplitude of vibration at the location X where it is largest, so that $|u_{d0}\,A|$ represents the amplitude of the dynamic axial displacement at the ZRB support.

The procedure used to account for the amplitude-dependent stiffness K_x and damping ratio ξ_{aB} is then as follows: (a) Pick a value for $|u_{d0}\,A|$. (b) Calculate K_x and ξ_{aB} from (24). (c) Calculate the analytical solution, as previously. (d) Calculate the amplitude of vibration for which the solution applies from $|A|=|u_{d0}\,A|/|u_{d0}|$. (e) Repeat these operations for different dynamic axial displacements at the support $|u_{d0}\,A|$ to generate the data for Figure 6.

The strong effect of nonlinearity and inelasticity of the axial resistance at the ZRB support is immediately clear from Figure 6. It has correspondingly strong implications for the in line VIV response of the span. The calculations only account for nonlinearity and inelasticity in axial resistance of the ZRB support. However, pluck tests on an operating pipeline [9] strongly suggest that other nonlinearity and inelasticity is also important. Including that in an FE model, leads to a nonlinear eigenvalue problem of the type solved in [10] for the simpler case of in line vibrations of a single span.

Another point of interest is the low sensitivity of the modal axial displacement at the ZRB support to the support stiffness K_x used in the analysis. This can be seen by substituting from (16) into the expression for the modal axial displacement u_d at the ZRB support in (15) to obtain

$$u_{d0} = g_d/\{1+ K_x/[2EA/(L+ \lambda_x)]\}\tag{25}$$

where g_d is given in (12). As expected, $u_{d0} = g_d$ when $K_x = 0$. Further, for the numerical example $[2EA/(L+ \lambda_x)]$=100.4 MN/m, and that is the stiffness K_x that would be needed at the ZRB support to reduce the modal displacement by 50%.

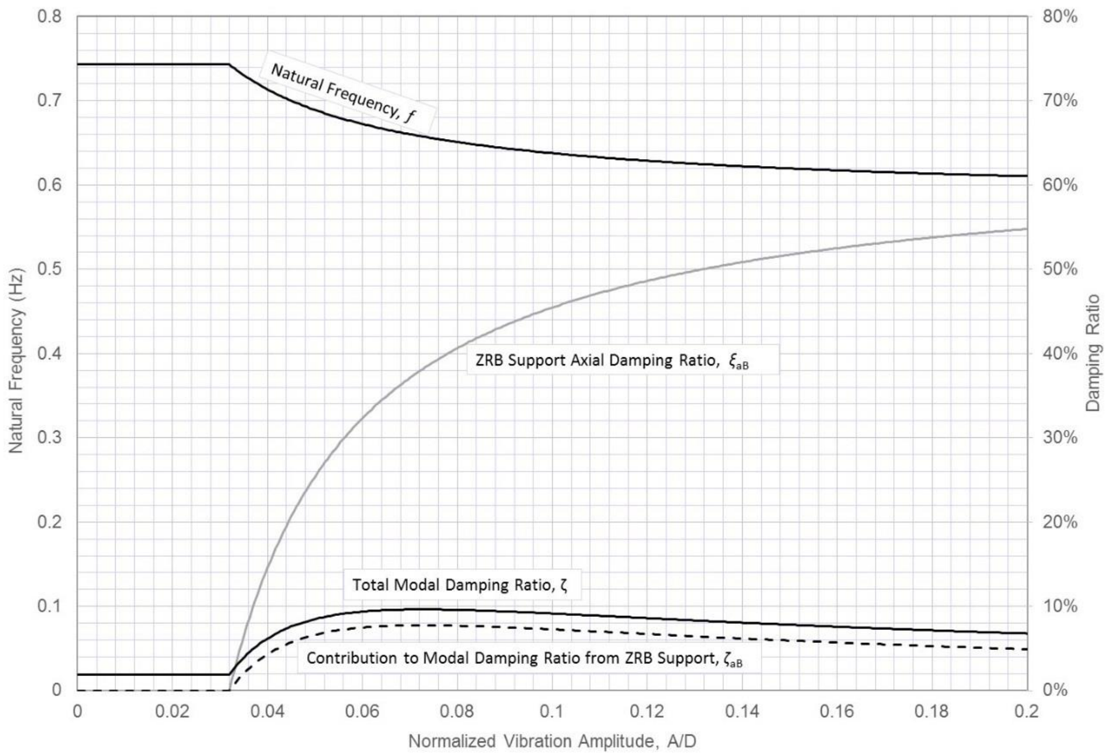

Figure 6 **Effect of nonlinearity and inelasticity on the first lateral mode, for an elastic-perfectly-plastic ZRB support with a mobilization displacement of 2mm, using amplitude-dependent linearization to determine the equivalent stiffness K_x and component damping ratio ξ_{aB} for the ZRB support in the axial direction. The axial dynamic displacement at the support $|A\ u_d|$ is 0 at *A/D*=0, 2mm at *A/D*=0.0319, 14.3mm at *A/D*=0.2, and varies linearly in between.**

6 Conclusions

The lateral mode for the spans of length L to each side of ZRB support under axially unconstrained conditions and neglecting axial inertia is the same as mode 2 for a straight pipe of length $2L$, and this is already available in [3].

However, the axial restraint at the ZRB support and the seabed together with the out-of-straightness due to lateral buckling on the ZRB support give rise to lateral arch action whereby the natural frequency is significantly raised. This effect is accurately captured by using the same Rayleigh-Ritz approximation as in [4].

In addition to being an analytical solution, the method presented has the advantages that: (a) Survey data can be used directly for the span lengths L and the static lateral out-of-straightness profile $y_s(X)$, (b) it gives a much clearer picture of importance of the stiffness and damping from the axial resistance at the ZRB support, and (c) it remains applicable if the pipe has been subject to plastic deformations, provided the correct static profile $y_s(X)$ is used as input to the analysis and the dynamic response does not involve additional yielding.

The results indicate that frictional axial slip at the ZRB support strongly influences the damping for this first in line (lateral) mode.

7 Acknowledgements

The author would like to thank the University of Western Australia (UWA), and in particular Phil Watson, Ali Karrech, Fraser Bransby, and others from the TIDE team there for the invitation to visit UWA, and many interesting and stimulating discussions and sharing of information during that visit, which lead to this revisiting of ZRB spans, for their dynamic behavior.

8 References

1. Atkins (2014) “SAFEBUCK JIP - Feedback from Operating Pipelines,” Atkins Report Number: 5087471.002.RP01.02, 10 November 2014.
2. Peek, R. , and Kristiansen, N. Ø., (2009), “Zero-Radius Bend Method to Trigger Lateral Buckles,” Journal of Transportation Engineering, Vol. 135, No. 12, December 1, 2009.
3. Sollund, H.A., Vedeld, K., Fyrileiv, O., (2015) “Modal Response of Free-Spanning Pipelines based on Dimensional Analysis,” Applied Ocean Research 50 (2015) 13-29.
4. Peek, R., Witz, M. and Vedeld, K. (2021) "Dynamics of a Pipeline Span on an Elastic Seabed," Applied Ocean Research 111 (2021) 102407.
5. Det Norske Veritas (2017) “Pipe-Soil Interaction for Submarine Pipelines,” Det Norske Veritas, Recommended Practice, DNVGL-RP-F114, May 2017, First Issue Edition.
6. Peek, R. (2016) “NPEX Finite Element Analysis Program Release,” by R. Peek, Shell Global Solutions, International, B.V., Report No. SR.16.12288, August 2016, Unrestricted. Available at www.peek.solutions.
7. Peek, R. (2022) “NPEX 22a Documentation Update,” Documentation of updates in the Npex FE Analysis Code, available at www.peek.solutions.
8. Det Norske Veritas (2017) “Free Spanning of Pipelines,” Recommended Practice DNVGL-RP-F105, June 2017 Edition, Amended September 2021.
9. Peek, R., Bernardo, C. A., Hong, H. M., O’Loughlin, C. D., White, D., & Ang, S. Y. (2020) “Pluck Tests on Operating Deepwater Pipeline Spans,” Engrxiv, DOI: https://doi.org/10.31224/osf.io/qypj7.
10. Peek, R. (2020) “Nonlinear Span Assessment by Amplitude-Dependent Linearization,” Journal of Offshore Mechanics and Arctic Engineering (JOMAE), ASME, Vol. 42, October 2020.